UNIVERSITY OF CALIFORNIA SAN DIEGO

Eversion and Retraction of a Soft Robot Towards the Exploration of Coral Reefs

A thesis submitted in partial satisfaction of the
requirements for the degree Master of Science

in

Engineering Sciences (Mechanical Engineering)

by

Jamie Luong

Committee in charge:

Professor Michael Tolley, Chair
Professor Ryan Kastner
Professor Tania Morimoto

2019

The thesis of Jamie Luong is approved, and it is acceptable in quality and form for publication on microfilm and electronically:

_____

_____

_____
Chair

University of California San Diego

2019

DEDICATION

This manuscript is dedicated to my family, friends, and mentors for believing in me and providing support throughout this graduate program. Their encouraging words during the most difficult times of this process kept me pushing forward to succeed.

EPIGRAPH

By three methods we may learn wisdom: First, by reflection, which is noblest; second, by imitation, which is easiest; and third by experience, which is the bitterest.

—Confucius

TABLE OF CONTENTS

LIST OF SUPPLEMENTAL FILES

The supplementary material for this manuscript includes the following:

File 1: luong_jamie_eversionrobot.mp4

File 2: luong_jamie_birchaquarium.mp4

LIST OF FIGURES

ACKNOWLEDGEMENTS

I would like to acknowledge Professor Michael Tolley for his support as the chair and main advisor of my committee. He has provided invaluable advice on technical challenges that have significantly helped me progress in my research project. Under his guidance, I have also developed myself professionally and personally throughout this master's program.

I would like to acknowledge Paul Glick for his mentorship, patience, and support in my research work and personal development. His encouragement has motivated me during the most challenging times in graduate school and his willingness to always help me learn has made me become a better engineer.

I would like to acknowledge Aaron Ong for his contributions to the initial design and tests for this research project. His assistance has helped me to progress the project forward.

I would like to acknowledge the Bioinspired Robotics & Design Lab (BRDL) for their advice, support, and wonderful company to work alongside with.

I would like to acknowledge collaborators from the Sandin Lab, including Dr. Stuart Sandin, Maya deVries, and Brian Zgliczynski for their input on the research project, especially with their expertise in the field of studying coral reefs.

I would like to acknowledge collaborators from the Kastner Lab, including Professor Ryan Kastner, Eric Lo, and Peter Tueller for their contributions in the algorithm for 3D model generation from video data collected with the robot.

I would like to acknowledge the UC San Diego Frontiers of Innovation Scholars Program (FISP) for supporting this research work.

Chapters 1-5, in part, have been accepted as a publication for the 2019 IEEE-RAS International Conference on Soft Robotics (RoboSoft). Jamie Luong, Paul Glick, Aaron Ong, Maya S. deVries, Stuart Sandin, Elliot W. Hawkes, and Michael T. Tolley were the primary co-authors of this paper.

VITA

2015	Bachelor of Science, University of California, San Diego
2019	Master of Science, University of California, San Diego

PUBLICATIONS

Luong J.*, Glick P.*, Ong A.*, deVries M. S., Sandin S., Hawkes E. W., Tolley M. T. (2019) "Eversion and Retraction of a Soft Robot Towards the Exploration of Coral Reefs", in 2019 IEEE-RAS International Conference on Soft Robotics (RoboSoft), *accepted.*

FIELDS OF STUDY

Major Field: Engineering Sciences (Mechanical Engineering)

Studies in Mechanical Engineering
Professor Michael Tolley

ABSTRACT OF THE THESIS

Eversion and Retraction of a Soft Robot Towards the Exploration of Coral Reefs

by

Jamie Luong

Master of Science in Engineering Sciences (Mechanical Engineering)

University of California San Diego, 2019

Professor Michael Tolley, Chair

Coral reefs are declining worldwide. Yet, critical information remains unknown about the basic biological, ecological, and chemical processes that sustain coral reefs because of the challenges to accessing their narrow crevices and passageways. A robot that grows from the tip through its environment would be well suited to this challenge as there is no relative motion between the exterior of the robot and its surroundings. In this thesis work, I present the design and development of an eversion robot for operation underwater, show that existing models work for constrained passageways if external contacts are taken into account, and introduce a new

model to describe the forces on the robot during retraction. Ambient water is used to pressurize the robot and maintain a neutral buoyancy. The robot operates in open loop without any steering, but can rely on its compliance to conform to natural crevices and pathways in its environment. The mechanism of eversion and retraction for an underwater soft robot is demonstrated as a potential approach for future non-destructive exploration of coral reefs.

Introduction

Figure 1: The natural crevices and passageways of the diverse coral reef structure present a challenge for accessing the internal structures non-destructively (Reef photo: M. Johnson).

Coral reefs are among the most biodiverse ecosystems in the world. Occupying less than 1% of the sea floor, coral reefs are home to more than 25% of all marine life [1][2]. However, the true biodiversity of the reef remains largely a mystery because current technology has limited the study of coral reefs primarily to their outer surfaces [2]. Filling the key knowledge gaps of the internal reef environment has become imperative as anthropogenic threats to the ocean, such as climate change and overfishing, drive the disappearance of healthy reefs worldwide [3]. Coral reefs are massive, three-dimensional structures with many tunnels and crevices that comprise the habitats of the reef matrix. These tunnels and crevices are estimated to be 30-75% of the reef habitat [4] and are thought to be critical for maintaining biological, ecological, and chemical processes [5][6][7]. However, the majority of reef species and the properties of coral habitats remain unexplored because of the difficulty of accessing internal reef structures non-destructively. Current knowledge of life in these cryptic habitats is based primarily on destructive sampling [2][8][9]. Aside from issues with destructive sampling to reef

health, the limitation of this method is the inability to provide in situ data on organismal ecology or biology.

The challenges of accessing delicate internal reef structures are due to factors including small and unpredictable spaces, rough surfaces, variable crevice diameters, irregular geometry, lack of light, difficulty of transmitting data underwater, and lack of prior knowledge on paths through reef cavities. Existing options to explore the reef matrix in situ are limited to either robotic instruments [10] or handheld endoscopic probes [11][12]. The Cave Cam, an endoscopic video camera, was the primary attempt to construct such a probe, but had limited ability in penetrating winding crevices since the head required manual control from the entrance. Controlling a probe is sufficiently challenging in low visibility, underwater habitats such that capturing useful data cannot be guaranteed. Together, these challenges motivate the need for a robotic system that can traverse the extreme spatial environment of the coral reef matrix. Accessing these reef habitats would allow biologists to document the behavioral and ecological characteristics of cryptic organisms and sample their abiotic environment.

Many of the robots designed to climb or swim through tortuous pathways are not well suited for the particular challenges of a coral reef. Robots that locomote with inchworm inspired motion rely on external contacts to brace themselves, but in a coral reef such contacts are available only intermittently [13][14]. Swimming robots are capable of navigating 3D space, but due to the size and communication constraints in the reef, these robots would need to be tethered to provide power and data transmission [15][16]. Any tether provides a significant constraint due to the high friction of dragging a cable through convoluted paths [17]. The emerging technology of eversion robots presents a compelling solution to this technical challenge. Eversion robots are a type of growing robot, characterized by their unique method of tip extension. Inspired by the biological process of growth, eversion robots are pressure-driven to deploy new material at their tip and lengthen their body (Fig. 2) [18][19][20][21][22]. Eversion robots are well suited to operate in small passageways and in delicate environments due to their

intrinsic compliance to conform to existing pathways [23][24][25]. Since these robots deploy material at the tip, there is no relative motion between the exterior of the robot body and its environment [18]. These growing robots are unencumbered by friction as the base of the robot body is static rather than sliding along a surface.

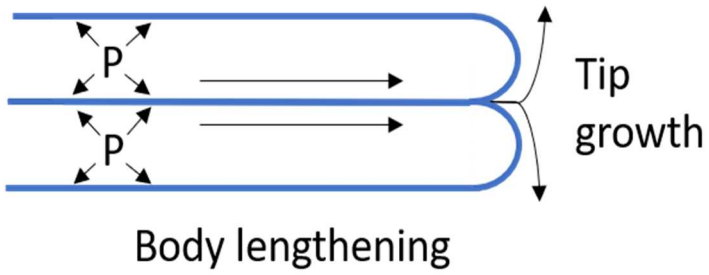

Figure 2: Eversion occurs upon applied pressure and extends the soft body by deploying new material at the tip.

Previous work has demonstrated the promise of eversion robots. Blumenschein et al. described the parameters that define the constraints on eversion [17]. Multiple studies have evaluated methods for position control of these soft robots and the maximum loads they can support [17][19][26]. However, retraction of an eversion robot has yet to be rigorously characterized. The deployed strength of these robots is greatly impacted by contacts with boundary constraints. Furthermore, eversion robots have proven to be well suited for operation in air, but have yet to be fully demonstrated in liquid environments (e.g. pipes, oceans).

The main contributions of this work are the design, implementation, and characterization modeling of a water-pressurized eversion robot. First, I present the design of an eversion robot, building upon the air-driven system developed in previous work, which is capable of underwater operation through using ambient water as the working fluid (Chapter 1). This section discusses practical design choices, as well as a change to the fluid control strategy due to the use of an incompressible liquid as the working fluid. Chapter 2 presents a new model to describe the forces during retraction of the robot, validates existing models, and addresses the behavior of

the robot operating in a confined space. Chapter 3 presents experimental results in comparison to the models. Chapter 4 presents demonstrations of the robot operation in small underwater tank tests and in a simulated field deployment of a coral reef environment. In Chapter 5, I provide concluding remarks and discuss potential future work.

Chapter 1: Design & Fabrication

The three main components in the design of this eversion robot are: a mechanical drivetrain, a rigid pressure chamber, and a soft body made of flexible fabric (Fig. 3). These components provide the necessary torque, pressure, and material for the growth mechanism. To operate underwater and collect visual data, additional designs were implemented to waterproof system components and to allow for a payload to be mounted at the robot tip.

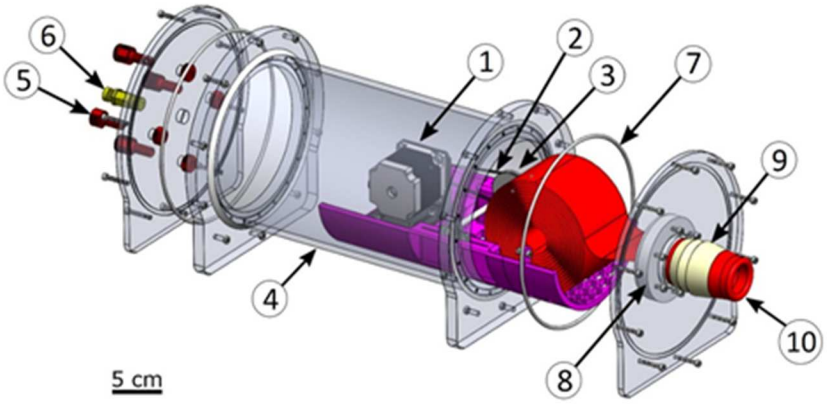

Figure 3: Exploded 3D model of the robot system. Mechanical drivetrain: 1) stepper motor, 2) timing belt, 3) pulley. Pressure chamber: 4) pressure chamber housing, 5) bolt penetrators, 6) pressure relief valve, 7) O-ring coated with grease, 8) bolted pressure seal adapter, 9) latex clamp. Soft robot body: 10) nylon fabric membrane.

1.1: Mechanical drivetrain

The mechanical drivetrain applies a torque to control the rates of extension and retraction during deployment of the system. A stepper motor, located inside a cylindrical pressure chamber, winches the spooled fabric body through a timing belt pulley system. The motor provides torque to counteract the pressure acting on the soft robot body and is remotely controlled with a microcontroller (Arduino Uno) to either spool or unspool the fabric. The radius of the spool with the wrapped fabric changes as the robot grows, which affects the torque output from the drivetrain. The use of a stepper motor eliminates the need for a feedback mechanism

to command the robot to a particular position. If the robot is depressurized and in a passageway, there is no tension along the fabric body and the robot will hold its position due to the passageway (Fig. 4). In this case, the power to the motor can be disconnected to save power on long duration deployments.

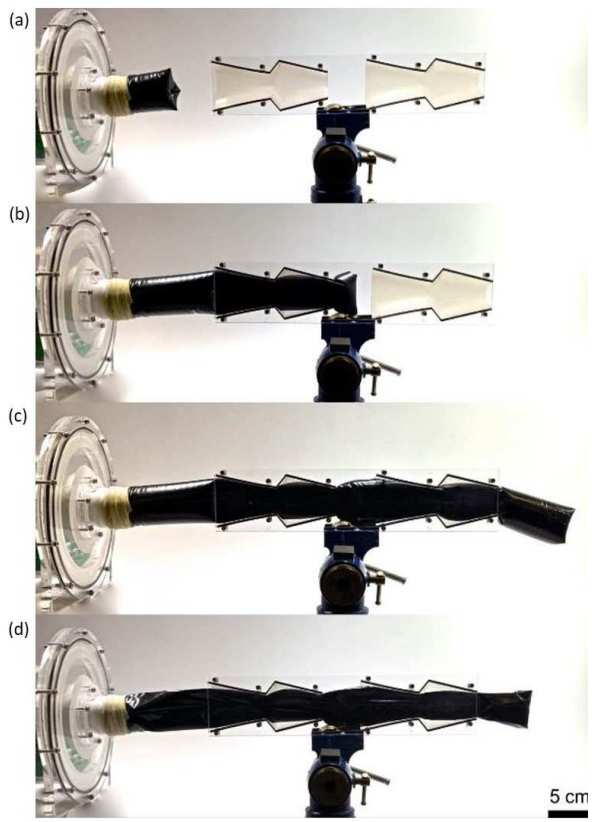

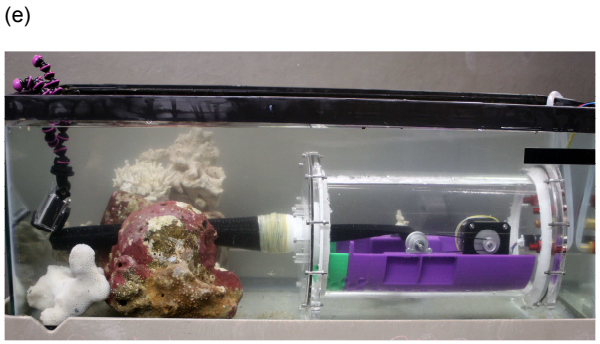

Figure 4: The robot can evert through varied passageways. This property makes these soft robots apt for operation in the highly variable coral reef matrix. (a) Robot at initial state before eversion. (b) Eversion through a constricting passageway. (c) Eversion proceeds through both passageways and free space. (d) The robot can enter a depressurized state to avoid blocking external flows or to conserve electrical power. (e) Due to its compliant nature, the robot can traverse through constrained environments, such as a coral reef matrix.

1.2: Pressure chamber

The pressure chamber provides internal pressure to drive the inflation and growth of the fabric body (Fig. 3). This pressure chamber is a sealed acrylic cylinder (16.5 cm diameter, 30.5 cm long) that houses all the components and connections. The rigid frame of the pressure chamber provides a secure mount for the drivetrain, electrical feedthroughs for the motor, and fluid connections used for the pump and pressure relief valve. At the front of the pressure chamber is a flange for the everted fabric body to be clamped against. The back plate contains bolt penetrators to connect to an external pump that supplies the fluid pressure and a relief

valve for self-regulation of the internal chamber pressure. Acrylic and 3D printed components allow for optical transparency and rapid prototyping, but would need to be replaced with corrosion-resistant metal parts for long-term field implementation.

1.3: Soft robot body

The soft body provides new material at the tip for the eversion mechanism. For material selection, a thin polyethylene film was initially used due to ease of implementation for the spool with pre-made tubing. However, after multiple trials of deploying the soft body, wrinkle propagation was observed in the material, increasing the tendency for the inflated body to buckle more easily. Heat-sealable nylon taffeta was the secondary material considered because of the ease of fabrication with a heat seal press. However, the high friction of the heat seal coating on one side of the material increased the required force to evert and retract.

To implement a soft body to withstand the eversion and retraction process, a flexible silicone and polyurethane coated ripstop nylon (Ripstop Nylon, Seattle Fabrics) was selected as the membrane material due to its waterproof properties and low coefficient of friction. The soft membrane body was fabricated using a layer of the silnylon fabric folded over onto itself to form a tube-like shape and mechanically stitched using a sewing machine. A thin layer of silicone adhesive (Silnet Seam Sealer, Gear Aid) was applied and cured at the seam to seal the body. This fabric body was clamped onto a 3D printed flange on the front plate of the pressure chamber to create a pressure-tight seal.

1.4: Designs for underwater operation

Eversion robots can be well suited to operating underwater, but this requires design and operational modifications. These robots use pressure to drive growth, and so must be designed as pressure-tight systems. With the exception of the pressure pump, most pneumatic-driven eversion robots [18][19] are already waterproof without modification. However, using air to drive

growth in a liquid medium will lead to large buoyancy forces acting along the body of the robot. Ideally, the fluid used to drive growth should have the same density as the fluid in the surrounding medium. For this application, I used surrounding water to make the robot neutrally buoyant and generate pressure for growth using a submersible pump.

However, the use of seawater inside the robot necessitates design changes to address three resulting challenges. 1) Liquids are generally incompressible, which complicates the pressure control for growth and retraction. 2) Electronics must be insulated from seawater, which is both conductive and corrosive. 3) All components, both inside and outside of the robot, need to withstand the marine environment.

Eversion using a liquid-filled robot occurs more slowly than with air since the working fluid is incompressible and cannot compress or adapt to the changing volume of the robot. The rate of growth is limited by the flow rate of the pump and the increased viscosity of the fluid. Retraction is also affected when using incompressible fluids because when the volume in the soft body decreases, the pressure in the chamber will increase significantly. Since water pumps provide only positive pressure, removing water from inside the robot to maintain a desired internal pressure presents a challenge for fluid control. I initially used a nylon passive pressure relief valve to enable retraction. Pressure relief valves open only when the pressure increases above the set-point threshold. This simple change allows the robot to easily release pressure for retraction in air, but requires significant time delay to depressurize when the robot is filled with water due to the higher internal pressure with an incompressible fluid. To enable better retraction underwater, an on-off pressure regulator valve was used to reduce internal pressure and increase fluid flow removal.

With seawater inside of the robot, electrical components need to be protected. The conductivity of saltwater does not short-circuit brushless motors (including stepper motors), but seawater can lead to undesirable corrosion and electrolysis. Commercially available stepper motors that are waterproof can be costly and limited in submersible depth and operation time.

To prevent motor corrosion, I fabricated a pressure-tight housing for the motor (Fig. 5). This 3D-printed housing has a soft diaphragm and is oil-filled to equalize pressure between the inside and outside of this housing. The oil is incompressible, electrically insulating, inert, and acts as a heat sink [33]. A rotary shaft seal was initially used to address the seal at the motor shaft to allow rotary motion, but was found to allow the inner fluid to leak into the main chamber and the outer environment over time due to the dynamic loads on the sealing element. Instead, a magnetic co-axial shaft coupling (MINEX-S, KTR), composed of an outer “driver” hub, inner “driven” hub, and containment shroud, was used to provide a better seal across the motor enclosure through a non-contact transfer of torque. The containment shroud creates a hermetic seal to the motor housing using an O-ring, creating a physical barrier between the inside and outside environments of the enclosure. The stepper motor controls the “driver” hub inside to magnetically transmit torque to the “driven” hub outside on the output shaft, which is connected to the timing belt system. Thus, this coupling component provides only static loads on the sealing elements while eliminating the need for contact between torque transmission parts. When implementing the magnetic shaft coupling with the motor housing design over several operations, no visible leaks were observed in the surrounding water.

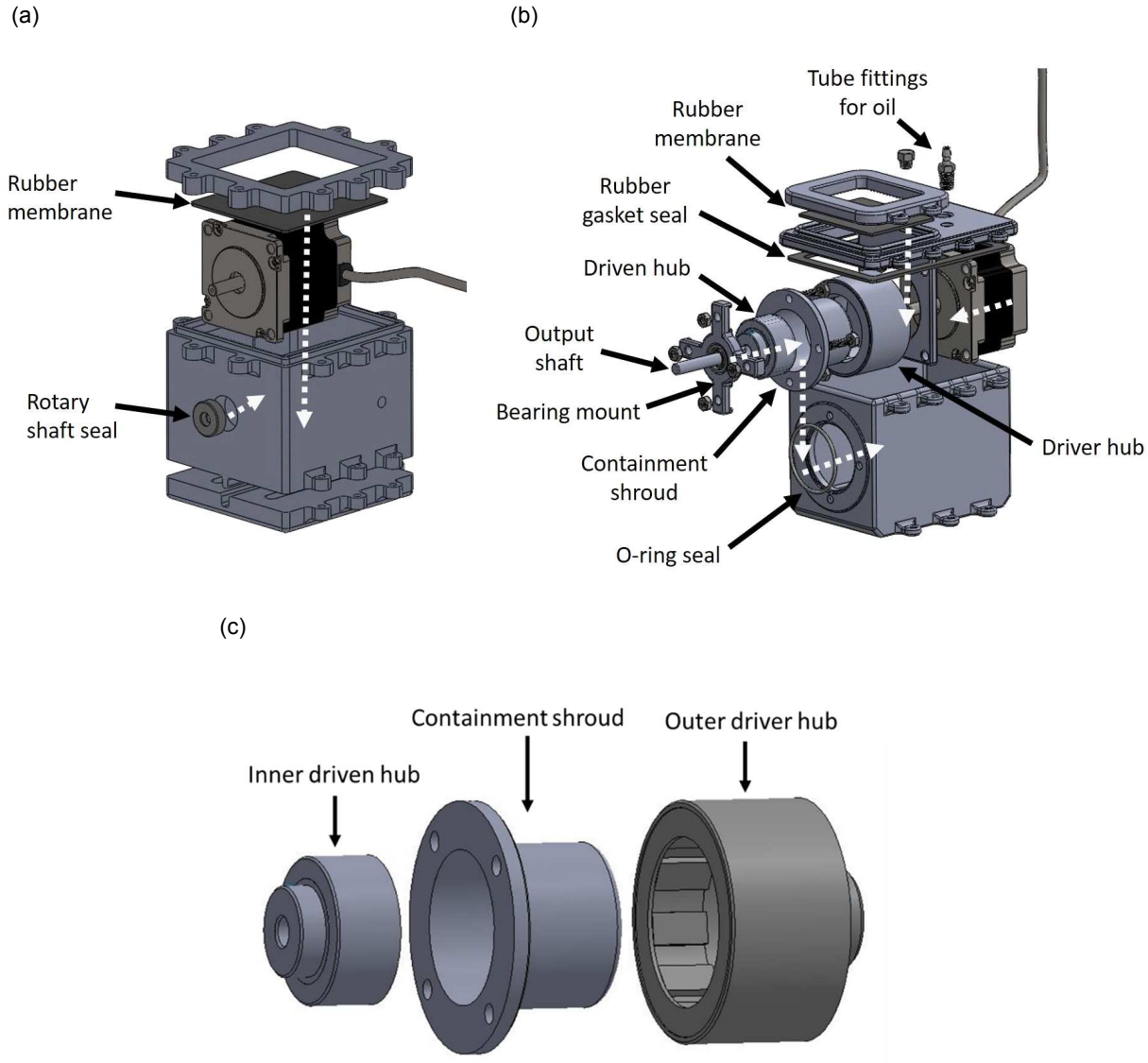

Figure 5: Motor housing design components. (a) Initial design of motor housing with rotary shaft seal and a flexible membrane for pressure equalization. (b) Final design of motor housing with magnetic shaft coupling to create a more sealed enclosure from seawater environment. (c) The magnetic co-axial shaft coupling is composed of three parts: 1) an inner driven hub with magnets placed along the outer cylinder, 2) a non-magnetic containment shroud, and 3) an outer driver hub with magnets placed along the inner side.

Finally, all components need to withstand the challenges of the marine environment, particularly corrosion, temperature fluctuations, biofouling, and hydrostatic stress. Passive mechanical components should be made of corrosion-resistant, temperature stable, and incompressible materials. For this prototype, several materials (acrylic, 3D printed plastics) were

used that are not suitable for long-duration or deep sea applications [35]. However, the depth of operation does not require significant modifications to the overall design of the robot other than material changes. Because each sealed area of the robot is filled with incompressible fluid and connected via soft membranes, the pressure differences (between the ambient water, interior of the robot, and motor housing) are on the order of several kilopascal, regardless of the depth of the robot (Fig 6). As such, the most significant forces on the robot will be hydrostatic stresses due to depth [34]. As long as the material of each component of the robot can withstand the hydrostatic stress associated with a particular depth, the actual depth of the robot does not necessitate change to the overall design or operation.

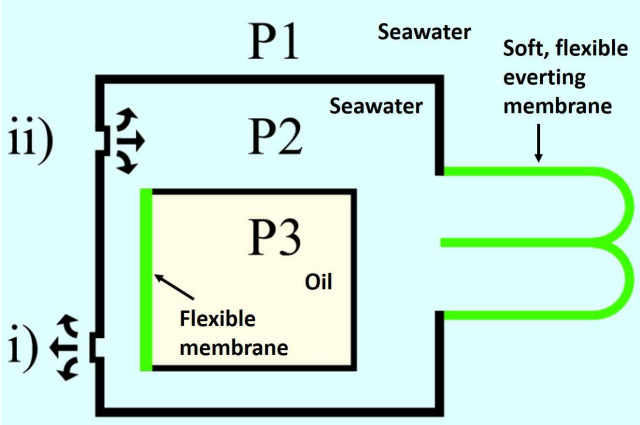

Figure 6: The pressure differentials between each chamber in the robot remain low, regardless of the ambient pressure (P1). A pump (ii) and pressure relief valve (i) regulate the internal chamber pressure P2 to be slightly higher than P1. The oil-filled motor housing has a flexible membrane, which maintains a minimal difference between its pressure P3 and P2.

1.5: Data collection payload

Prior eversion robots can support payloads to collect scientific data, such as a camera or water-sampling device, but typically require tethers to support devices at the growing tip [18]. A new untethered payload mechanism was implemented at the tip using ring magnets (Fig 7). This tip device was comprised of two parts, one inside and one outside of the fabric body. The inside piece was a torus with the fabric inserted through the center hole which keeps the

mechanism centered at the tip. The ring magnets allowed the fabric material to slide along inner and outer parts of the tip mount as the soft body grows. A small waterproof camera was mounted onto this magnetic device at the tip to record video data as the robot everts. To guarantee recovery of the payload in the case that the inner and outer parts get disconnected during deployment, a backstop connected to the outer mount and placed through the inner hole of the torus was implemented to prevent loss of the payload.

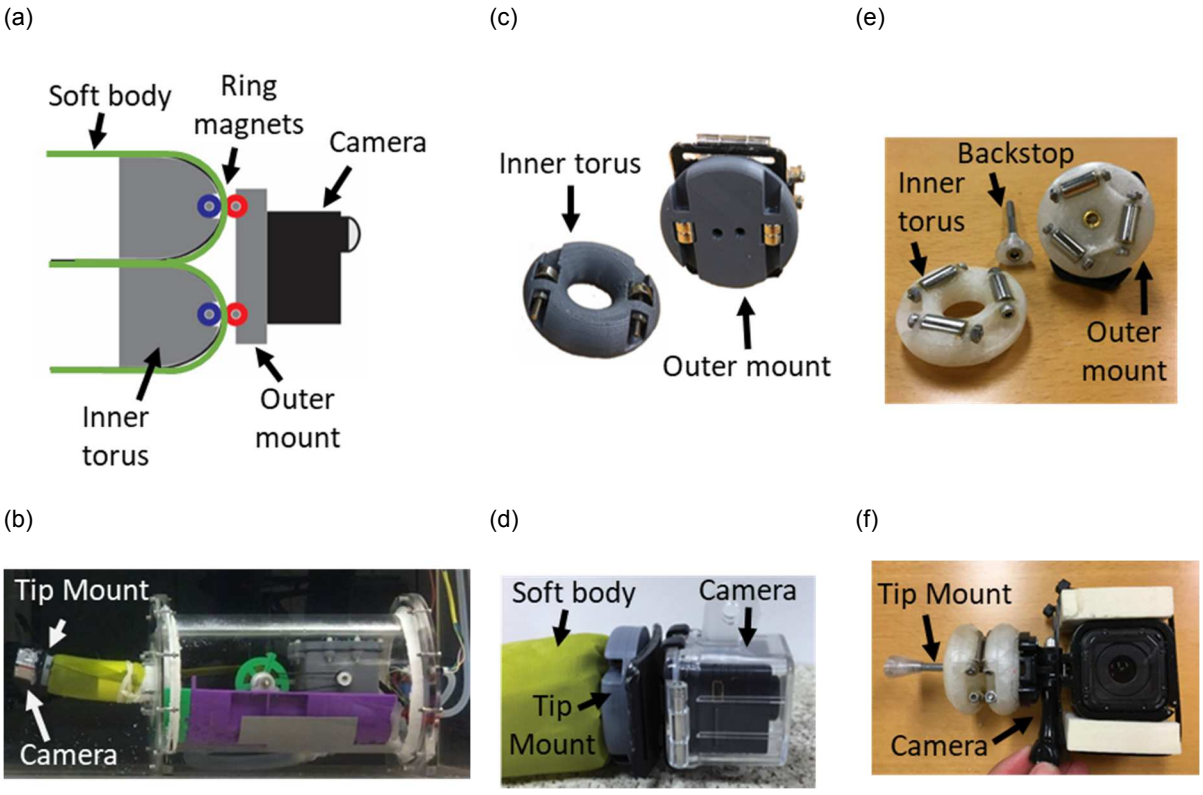

Figure 7: Data collection payload. (a) A cross section of the magnetic mechanism to support a payload at the robot tip. (b) Using a torus inside the robot keeps the mechanism constrained along the axis of growth. (c-d) Free-spinning ring magnets allow the fabric to slide between the inner and outer parts. The rigid plate can support payloads, such as a small camera, with the soft fabric body inserted through the torus. (e-f) A backstop interlocks with the outer mount through the inner torus to recover payloads at the tip.

Chapter 2: Modeling

We present models for the behavior of eversion robots in constrained environments. When the robot everts a particular length, it is useful to look at the forces the robot can withstand until failure to test its robustness and limits of operation. We also consider the parameters that affect the required force to allow retraction of the robot body after eversion.

2.1: Loading on the Robot

We describe models for the loading conditions with eversion robots. Load bearing capability in free space has been well modeled for inflatable beams and eversion robots pressurized by air [17][19][27][28]. We briefly review these results for both the case of axial and radial loading cases. Axial buckling describes the maximum compressive force an inflatable beam can withstand before failure [27]:

$$F_{axial} = \frac{EI\frac{\pi^2}{L^2}(B+G\pi rt)}{EI\frac{\pi^2}{L^2}+B+G\pi rt} \quad (1)$$

where r is the radius of the everted tube, E is Young's modulus, I is the area moment of inertia for a cylindrical shell, L is the length of the beam, B is the axial force due to internal fluid pressure P, G is the shear modulus, and t is the cylindrical wall thickness. The maximum radial load for an eversion robot in free space is also well described by inflatable beam theory [19][26][29][30]. Failure under transverse load occurs by wrinkle propagation and bending of the beam. The maximum radial force of an inflatable beam is described by Eq. 2 and the moment by Eq. 3 [30].

$$F_{radial} = \frac{\pi p r^3}{L} \quad (2)$$

$$M_{bending} = \pi p r^3 \quad (3)$$

However, these models for critical loads need to account for external contacts along the length of the soft membrane in a constriction or along a passageway. These boundary constraints can impact the maximum loads of the robot. We demonstrate how these models can be extended for behavior with constrictions in Chapter 4 Experimental Results section.

2.2 Effect of Friction and Path on Retraction

Friction occurs between the inner layers of the soft membrane body in a bend and is an important parameter for modeling eversion and retraction in a constrained environment (Fig. 8a, 8b). Modeling this friction establishes mechanical requirements for the drivetrain of an eversion robot given a coefficient of friction, pressure in the robot, and particular path. These models help describe the maximum forces that eversion robots can exert on their path, which is relevant for guaranteeing non-destructive exploration of sensitive coral. While the tension required to initiate retraction at the tip of the robot may be readily found, the matter is complicated by friction, which is dependent on the path of the robot. The magnitude of axial force exerted by the internal pressure is simply the pressure P times the cross-sectional area A of the soft body. Under static conditions, a force balance yields Eq. 4.

$$T_i + T_o = PA \qquad (4)$$

Exerting a tension at the tip $T_i > \frac{PA}{2}$ may initiate retraction, but the required force should also depend upon friction and the path taken by the robot. Based on Euler's formula for belt friction, the drivetrain of the winch motor must apply a force [31]:

$$F_{drivetrain} = (\frac{PA}{2})e^{\gamma\mu} \qquad (5)$$

where μ is the coefficient of friction of the tube material against itself, and γ is the total contact bend angle across the everted length. As illustrated in Fig. 8b, the bend angle γ_i depends on each contact along the robot's path in the environment. In this way, the force required to

guarantee retraction may be found. For a spooled membrane, the torque supplied by the drivetrain depends on how much spooled material remains as this affects the gear ratio [19]. While the drivetrain force increases exponentially as a function of the total bend angle γ, the pressure P in the robot may be lowered and the tube material may be selected with low-friction coating μ to ease the retraction process.

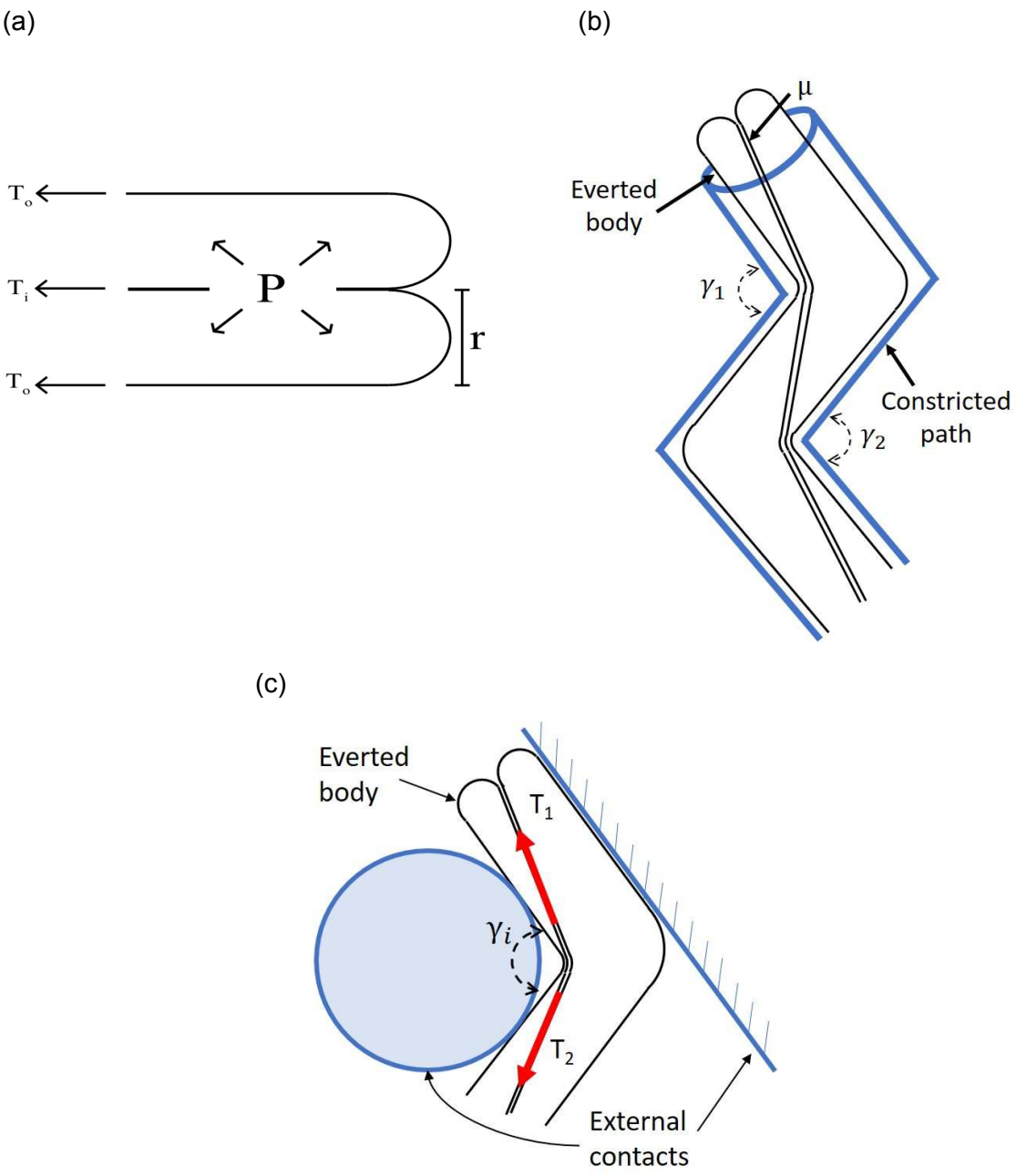

Figure 8: Force required for retraction depend on applied pressure and friction. (a) Cross-sectional side view of the free body diagram of the tip of the robot. P describes the internal pressure and T_i and T_o are the inner and outer tensional force acting on the material. (b) The sum of all individual γ_i is the total bend angle of the everted body for all external contacts in the robot's path. (c) Belt tension across a bend due to external contacts is shown by holding force T_1 and pulling force T_2. The reaction force on the environment from the retraction process is dependent upon the contact angle γ_i.

2.3 Reaction forces on environment

While it may be possible to guarantee retraction with a sufficiently powerful drivetrain, we present two models to evaluate the force of an eversion robot on its environment during the retraction process. We seek to model the pressure that the robot exerts on the objects with which it comes in contact, and model the reaction forces on an environment that arise from the tension in the robot (Fig. 8c). While Eq. 5 evaluates the robot path as a whole, these models instead concern each individual bend within the robot path. For this reason we generalize the tension on each side of a bend to be T_1 and T_2, defined such that $T_1 < T_2$ (i.e. friction is acting to resist motion towards T_2), the angle of a particular bend as γ_i, r as the radius of the soft robot body, and C as the radius of curvature of the bend. Eq. 6 describes the maximum contact pressure ρ_0 across a bend angle γ_i [31].

$$p_0 = \frac{T_1}{2rC} \qquad (6)$$

The magnitude of the reaction force on a bend may be found with [31]:

$$\left||F_{reaction}|\right| = \sqrt{T_1^2 + T_2(\gamma_i)^2 - T_1 T_2(\gamma_i) cos(\gamma_i)} \qquad (7)$$

where $T_2(\gamma_i)$ is defined by Euler [32]:

$$T_2(\gamma_i) = T_1 e^{\gamma_i \mu} \qquad (8)$$

Using these equations with knowledge of the path of the robot, it may be possible to fully describe the reaction forces and local pressures on the environment through which the robot has everted. With enough fluid pressure and motor torque, the robot may evert long distances through winding passageways. These equations provide further tools to model the forces from eversion and retraction on the pathway itself.

Chapter 3: Experimental Results

We conducted experiments to validate the models for loading conditions presented in Chapter 2. In the experiments for axial and radial loading, we used air as the working fluid to draw comparison to existing models and show the impact of boundary constraints. We determined the optimal pressure for retraction of the eversion robot.

3.1: Loading on the Robot

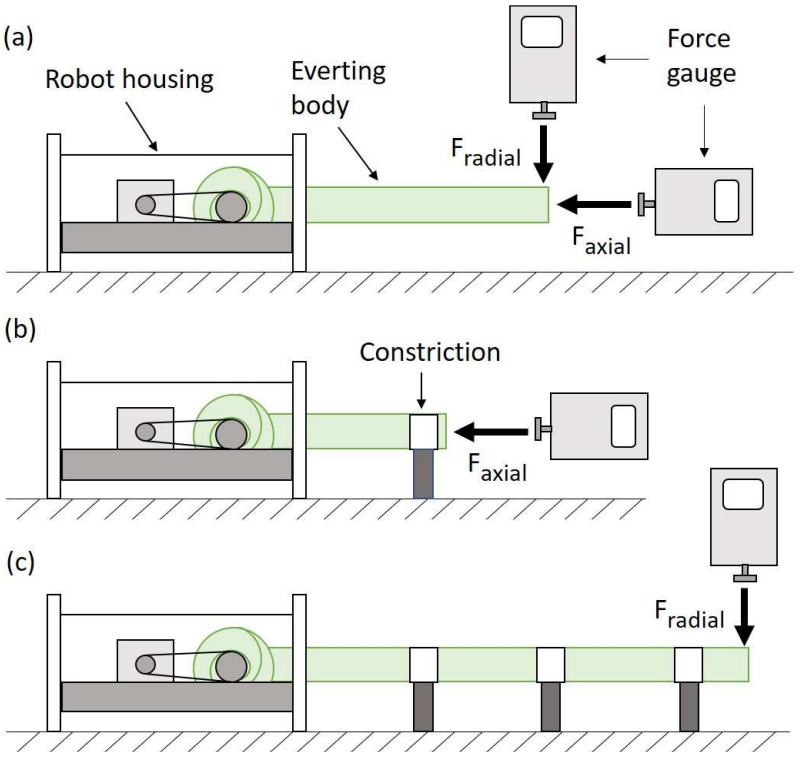

Figure 9: Experimental setup for measuring maximum loads of the everted soft body. Axial and radial loads were measured in (a) free space and (b-c) with constrictions. Measurements were performed using a force gauge and applying a force in the axial and radial directions as shown until failure occurred.

3.1.1: Axial Loading

The maximum axial force is dependent upon the pressure applied. Thus, we varied the pressure inside the robot and held the beam at a constant length of 30 cm, applying an increasing load axially until failure occurred both in free space and in a cylindrical constriction

with a radius smaller than the body of the robot (Fig. 9a-b). To measure the axial load, we recorded the force required to deflect the tip 3 mm, which was determined as the failure point across varied pressures. Measurements were taken with a force gauge (Mark 10 M3-20), and each data point represents the average of five trials (Fig. 10). We evaluated the model using two different radii for the soft body. Radii A and B were 1.6 cm and 2.4 cm, respectively. To generate the model, we used G = 0.742 MPa, determined experimentally. The membrane material was nylon taffeta with 0.16 mm thickness. Fig. 10 shows that the experimental data when the robot is in free space is well approximated by the model and agrees with prior results [19]. However, the failure mode of the robot depends on the effective length. Shorter beams tend to fail due to crushing rather than buckling. With a short enough effective length (i.e. in a constriction), the failure mode of eversion robots shifts from buckling to crushing. Constrictions serve to shorten the effective length of the robot and thereby change the failure mode and increase the maximum axial force. Because the outer membrane is flexible, failure is not catastrophic and is reversible once the load is removed.

3.1.2: Radial Loading

We experimentally validated that Eq. 3 describes the maximum bending moment in an eversion robot. Importantly, passageways provide a mechanical reinforcement that effectively shortens the moment arm. To collect the data, we deployed the robot with a radius of 2.4 cm operating at 10 kPa and measured radial load at periodic lengths up to 0.8 m. Measurements were taken with a force gauge (Mark 10 M3-20), and each data point represents the average of five trials. We then measured the radial force as we deployed the robot through a series of constrictions positioned along the length of the beam (Fig. 9c). In comparison with radial load measurements in free space, we observed that the constrictions effectively reset the length of the beam. A result of Eq. 2 is that the maximum radial load before failure does not depend on the overall length of the robot, but instead depends on the moment arm of the applied load. The

moment arm of a load applied radially at the tip of the robot may be taken as the total everted length since the contact with the last constriction. We model this behavior and show these results in Fig. 10.

(a)

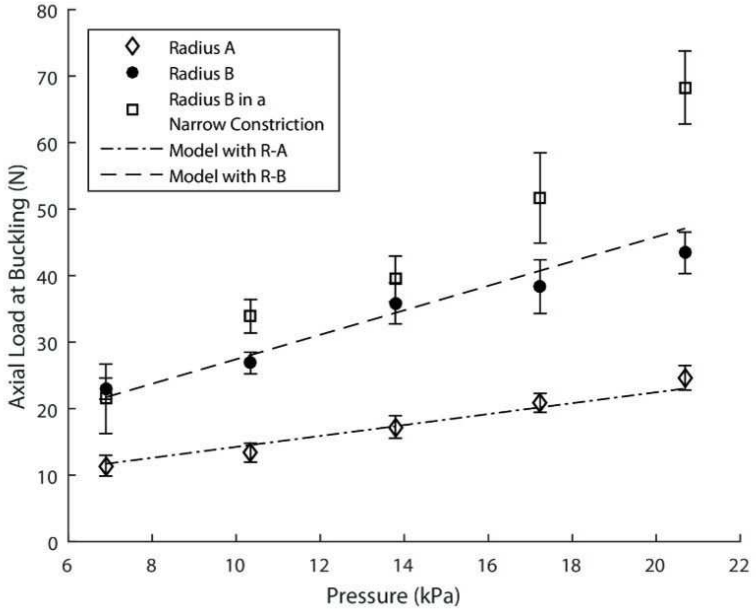

(b)

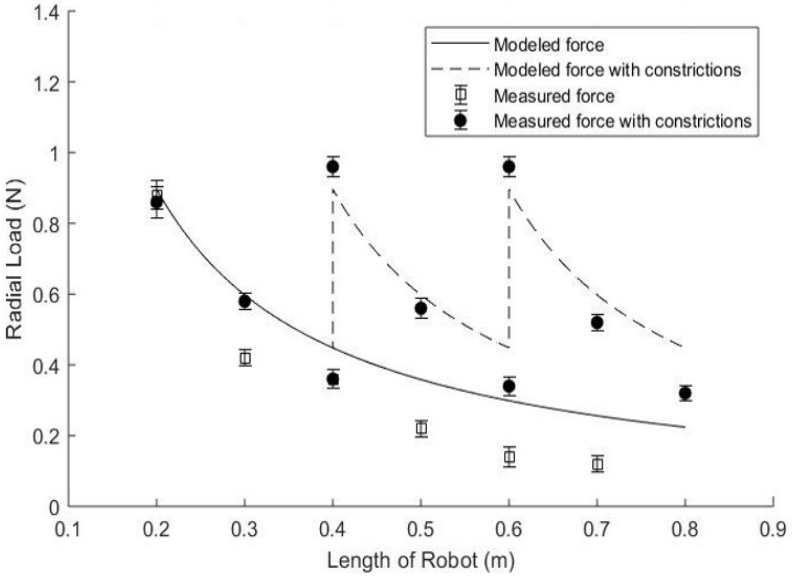

Figure 10: Results for maximum axial and radial loads. (a) Relationship between internal pressure and axial load at failure. The passageway acts as a boundary constraint, shortens the effective length of the robot, and increases its axial load. (b) Maximum radial force depending on the everted length of robot body. When the robot passes through periodic constrictions, the effective moment arm of the load is shortened.

3.2: Effect of Friction and Path on Retraction

Equations 5, 6, and 7 help quantify both the effect of friction and the path taken on the robot and the impact on its environment, which can influence design requirements of the robot. Pressure may be reduced to ease retraction, but there is a minimum pressure at 3.5 kPa beneath which the everted membrane loses shape. By selecting a material with a low coefficient of friction (silicone and polyurethane coated nylon), which was experimentally determined to be $\mu = 0.25$ for silnylon, retraction becomes much easier. For a given drivetrain and friction of material selected in the design of the robot, we demonstrate the dependence of friction and the path on the force to retract. We everted the robot through constrictions of varied contact angles from 0 to π radians at a constant pressure of 8.7 kPa. Using a digital pressure gauge (Solar Metrix), the maximum internal pressure to allow retraction was measured and averaged over three trials.

We found that as the contact angle increased, the required pressure had to be lowered such that the tension from the drivetrain was sufficient to overcome the friction and path-dependent forces to retract (Fig. 11). These results validate the exponential relationship described in Eq. 5 between the path-dependent contact angle and pressure to allow retraction.

(a)

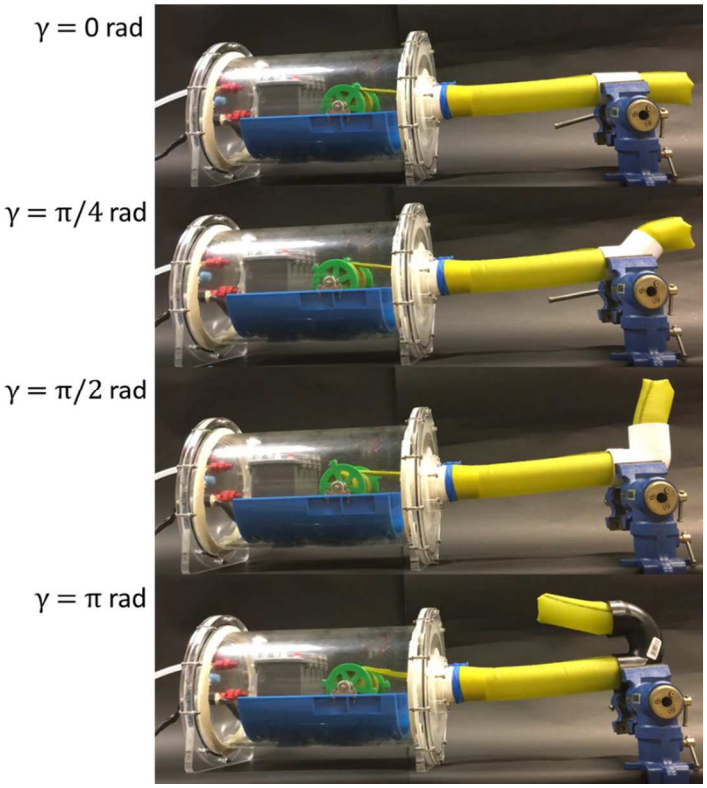

(b)

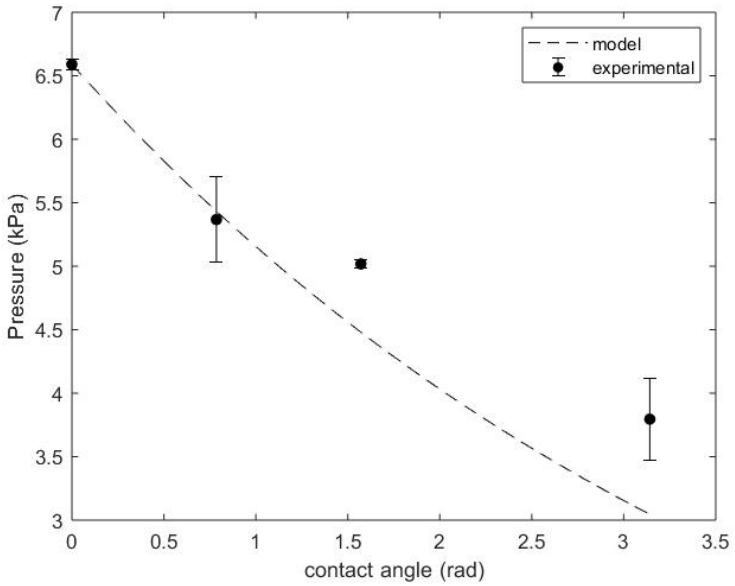

Figure 11: Results for effect of friction and path on robot retraction. (a) The robot everts through constrictions of varying contact angles γ from 0 to π radians. Pressure for the robot to retract was measured across the conditions over three trials. (b) When the contact angle increased, the maximum internal pressure in the robot had to be lowered to allow retraction.

Chapter 4: Underwater Demonstration and Tests

An underwater demonstration was performed in small tank tests to show the design implementation and behavior of the eversion robot. Data collection was achieved with the camera mounted with the magnetic mechanism at the robot tip. Deployment of the eversion robot in a simulated coral reef environment at the Birch Aquarium showed potential for the ability to non-destructively study within crevices and constrained passageways of coral reef structures in the field.

4.1: Underwater demonstration in small tank

To demonstrate eversion underwater, we implemented waterproof components and applied a constant pressure with a small submersible pump. We pressurized the internal chamber with surrounding water to drive the robot. Excess fluid pressure within the vessel was released through the relief valve outlet, with a set pressure of 20 kPa, to maintain constant internal pressure. Additionally, a small waterproof camera was attached at the robot tip with a magnetic payload adapter. With neutral buoyancy, the eversion robot may deploy large lengths of unsupported material without buckling due to its own weight, a behavior that is more challenging in air. Using water as the working fluid, the robot everted at a rate of 1 cm/s. As compared to air, the growth rate was decreased by about 7 times due to the incompressibility of water and the limited flow rate of our pump.

In this demonstration, we conducted several qualitative experiments. We showed successful eversion and retraction underwater and through constrictions in small tank tests (see supplementary video). We also presented the capability for underwater data collection with a camera mounted at the tip (Figure 12). The video footage of an object in the everted path captured from camera at the robot tip was then reconstructed into an initial 3D model through an image processing algorithm. This demonstrates initial steps towards the potential for acquiring data underwater to generate 3D models of coral reefs for field deployment.

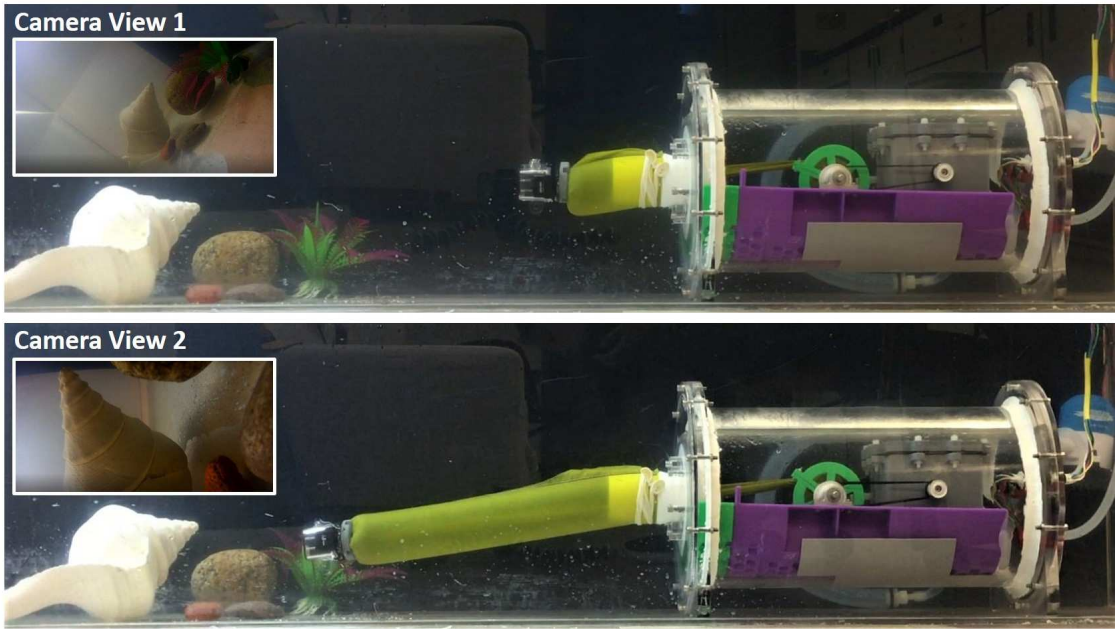

Figure 12: Demonstration of eversion underwater. The main chamber of the robot was flooded with water and pressurized to drive the eversion process. Using water instead of gas creates a neutrally buoyant robot. An untethered camera attached at the tip allows for data collection as the robot moves along a path. Images 1 and 2 capture the side view of the robot and the camera's point-of-view in the initial (top) and final (below) positions as the robot everts towards an object.

4.2: Deployment in a coral reef environment

Following small underwater tank tests, the eversion robot was then deployed in a coral reef environment tank at the Birch Aquarium at the Scripps Institute of Oceanography (SIO), with the goal of acquiring video transects of passageways within the reef structures (Fig. 13). Off-board electronics were used to remotely control the eversion and retraction from above the tank. Given the tank depth of 5 m and the limited length of the pump power cord, the length of tubing to supply pressure was scaled, which reduced the overall flow rate from the submersible pump. The lower flow rate from the pump was observed to amplify the time delay for pressurizing the volume of the soft body as new material deployed at the tip during eversion. Thus, the water pump was replaced with a higher rating (from 2.3 m^3/hr to 6.4 m^3/hr at initial flow rate) to allow for continuous growth of the soft body. To enable retraction, the pump was turned off and the regulator valve was turned on to release pressure for reducing the necessary

drivetrain force. To collect video transects of the coral reef structures, a small waterproof camera (GoPro Hero4 Session) was mounted at the tip, with the addition of syntactic foam (BlueRobotics) to keep the payload neutrally buoyant.

Scaling the robot system for deployment in a simulated coral reef environment presented a few challenges during the tank tests. While the robot was able to evert with the tip mount mechanism upon sufficiently applied pressure, the increased friction in sliding between the mount and the fabric material became challenging for retraction. With the reduced force due to lowered pressure for retraction, the drivetrain force was unable to overcome the frictional force from the tip mount without external assistance from a diver to disconnect the outer mount. Acquiring qualitative video transects of the coral reef matrix for rendering a 3D model also proved to be a difficult task due to the lack of active directional control. In future work, we intend to address these issues to improve the robot to operate in field deployment. Redesigning the camera tip mount to reduce friction can ease sliding of the fabric body to retract. Additionally, implementing tendon-driven actuation or series of pouch motors along the soft body can allow for directional control of the tip to obtain more reliable data during transects [26].

(a)

(b)

Figure 13: The eversion robot was tested in a coral reef tank at Birch Aquarium in SIO. (a) A diver assisted in the deployment of the robot to collect data of coral reef structures. (b) The base chamber of the body remains stationary, while the soft fabric body is able to grow through the passageways of coral reefs with the goal of acquiring transects to translate the structures into 3D models for studying the health and ecology of various species.

Chapter 5. Conclusions and Future Work

Pressure-driven and compliant, eversion robots hold significant promise for navigating twisting, tortuous passages. The external bodies of these robots do not slide relative to surroundings, can access complex pathways, and do not depend on a continuous external contact to support or guide forward motion. These properties are in contrast to many prior robotic explorers, and have a wide range of applications including exploration in coral reefs, inspection of mine shafts, and navigation in cavities of the human body.

In this work, we showed existing models can be adapted to account for behavior with contacts along the body of the robot. Additionally, retracting or recovering the robot is a non-trivial task, and we present a model to describe the forces during retraction. We implemented a pressure control and design approach for eversion robots that operate underwater. Furthermore, we demonstrated the robot operating underwater in small tank tests and through constrained passageways in a coral reef environment. Integrating a camera mounted at the tip allowed for data collection, which showed the potential to render 3D models of coral reef matrices in future field deployment to study their health and ecology.

Future work may include optimizing retraction methods with a payload at the tip, providing directional control, and distributed sensing on the soft body to map the coral reef. Innovations presented in this work are a step towards a field-capable eversion robot for non-destructive exploration of the internal coral reef structures.

Chapters 1-5, in part, have been accepted as a publication for the 2019 IEEE-RAS International Conference on Soft Robotics (RoboSoft). Jamie Luong, Paul Glick, Aaron Ong, Maya S. deVries, Stuart Sandin, Elliot W. Hawkes, and Michael T. Tolley were the primary co-authors of this paper.

References

[1] M. L. Reaka-Kudla, “The global biodiversity of coral reefs: a comparison with rain forests,” Biodiversity II: Understanding and protecting our biological resources, vol. 2, p. 551, 1997.

[2] L. Plaisance, M. J. Caley, R. E. Brainard, and N. Knowlton, “The diversity of coral reefs: what are we missing?,” PLoS One, vol. 6, no. 10, p. e25026, 2011.

[3] J. M. Pandolfi, S. R. Connolly, D. J. Marshall, and A. L. Cohen, “Projecting coral reef futures under global warming and ocean acidification,” science, vol. 333, no. 6041, pp. 418–422, 2011.

[4] R. N. Ginsburg, “Geological and biological roles of cavities in coral reefs,” Perspectives on coral reefs. Australian Institute of Marine Science, Townsville, pp. 148–153, 1983.

[5] M. Depczynski and D. R. Bellwood, “The role of cryptobenthic reef fishes in coral reef trophodynamics,” Marine Ecology Progress Series, vol. 256, pp. 183–191, 2003.

[6] J. M. de Goeij and F. C. Van Duyl, “Coral cavities are sinks of dissolved organic carbon (doc),” Limnology and Oceanography, vol. 52, no. 6, pp. 2608–2617, 2007.

[7] J. M. De Goeij, D. Van Oevelen, M. J. Vermeij, R. Osinga, J. J. Middelburg, A. F. de Goeij, and W. Admiraal, “Surviving in a marine desert: the sponge loop retains resources within coral reefs,” Science, vol. 342, no. 6154, pp. 108–110, 2013.

[8] I. C. Enochs, L. T. Toth, V. W. Brandtneris, J. C. Afflerbach, and D. P. Manzello, “Environmental determinants of motile cryptofauna on an eastern pacific coral reef,” Marine Ecology Progress Series, vol. 438, pp. 105–118, 2011.

[9] M. Kramer, D. Bellwood, and O. Bellwood, “Benthic crustacea on coral reefs: a quantitative survey,” Marine Ecology Progress Series, vol. 511, pp. 105–116, 2014.

[10] S. R. Scheffers, J. de Goeij, F. C. van Duyl, and R. P. Bak, “The caveprofiler: a simple tool to describe the 3-d structure of inaccessible coral reef cavities,” Coral Reefs, vol. 22, no. 1, pp. 49–53, 2003.

[11] M. Wunsch and C. Richter, “The cavecam—an endoscopic underwater videosystem for the exploration of cryptic habitats,” Marine ecology progress series, pp. 277–282, 1998.

[12] C. Richter, M. Wunsch, M. Rasheed, I. Ko`Etter, and M. I. Badran, “Endoscopic exploration of red sea coral reefs reveals dense populations of cavity-dwelling sponges,” Nature, vol. 413, no. 6857, p. 726, 2001.

[13] J. M. Friesen, P. Glick, M. Fanton, P. Manovi, A. Xydes, T. Bewley, and V. Sunspiral, “The second generation prototype of a duct climbing tensegrity robot, ducttv2,” in Robotics and Automation (ICRA), 2016 IEEE International Conference on, pp. 2123–2128, IEEE, 2016.

[14] M. S. Verma, A. Ainla, D. Yang, D. Harburg, and G. M. Whitesides, “A soft tube-climbing robot,” Soft robotics, vol. 5, no. 2, pp. 133–137, 2018.

[15] J. Yuh, “Design and control of autonomous underwater robots: A survey,” Autonomous Robots, vol. 8, no. 1, pp. 7–24, 2000.

[16] D. Ruffatto, P. E. Glick, M. T. Tolley, and A. Parness, “Longduration surface anchoring with a hybrid electrostatic and geckoinspired adhesive,” IEEE Robotics and Automation Letters, vol. 3, no. 4, pp. 4201–4208, 2018.

[17] L. H. Blumenschein, A. M. Okamura, and E. W. Hawkes, “Modeling of bioinspired apical extension in a soft robot,” in Conference on Biomimetic and Biohybrid Systems, pp. 522–531, Springer, 2017.

[18] E. W. Hawkes, L. H. Blumenschein, J. D. Greer, and A. M. Okamura, “A soft robot that navigates its environment through growth,” Science Robotics, vol. 2, no. 8, p. eaan3028, 2017.

[19] Z. M. Hammond, N. S. Usevitch, E. W. Hawkes, and S. Follmer, “Pneumatic reel actuator: Design, modeling, and implementation,” in 2017 IEEE International Conference on Robotics and Automation (ICRA), pp. 626–633, May 2017.

[20] A. Sadhegi, A. Tonazzini, L. Popova, and B. Mazzolai, “A novel growing device inspired by plant root soil penetration behaviors,” in PLOS ONE, vol. 9, 2014.

[21] I. W. SCUDAMORE, B. C. DUNPHY, and I. D. COOKE, “Outpatient falloposcopy; intra-luminal imaging of the fallopian tube by transuterine fibre-optic endoscopy as an outpatient procedure,” BJOG: An International Journal of Obstetrics & Gynaecology, vol. 99, no. 10, pp. 829–835, 1992.

[22] T. Rosch, A. Adler, H. Pohl, E. Wettschureck, M. Koch, B. Wiedenmann, and N. Hoepffner, “A motor-driven single-use colonoscope controlled with a hand-held device: A feasibility study in volunteers,” in Gastrointest. Endosc., vol. 67, pp. 1139—-1146.

[23] D. Rus and M. T. Tolley, “Design, fabrication and control of soft robots,” Nature, vol. 521, no. 7553, p. 467, 2015.

[24] P. Glick, S. Suresh, D. Ruffatto III, M. Cutkosky, M. T. Tolley, and A. Parness, “A soft robotic gripper with gecko-inspired adhesive,” IEEE Robotics and Automation Letters, 2018.

[25] P. Polygerinos, N. Correll, S. A. Morin, B. Mosadegh, C. D. Onal, K. Petersen, M. Cianchetti, M. T. Tolley, and R. F. Shepherd, “Soft robotics: Review of fluid-driven intrinsically soft devices; manufacturing, sensing, control, and applications in human-robot interaction,” Advanced Engineering Materials, 2017.

[26] J. D. Greer, T. K. Morimoto, A. M. Okamura, and E. W. Hawkes, “Series pneumatic artificial muscles (spams) and application to a soft continuum robot,” in Robotics and Automation (ICRA), 2017 IEEE International Conference on, pp. 5503–5510, IEEE, 2017.

[27] W. Fichter, “A theory for inflated thin-wall cylindrical beams,” 1966.

[28] C. Wielgosz and J.-C. Thomas, “An inflatable fabric beam finite element,” International Journal for Numerical Methods in Biomedical Engineering, vol. 19, no. 4, pp. 307–312, 2003.

[29] Y. He and W. Chen, “Experiment and theoretical analysis study of etfe inflatable tubes,” International Journal of Aerospace Engineering, vol. 2014, 2014.

[30] R. Comer and S. Levy, “Deflections of an inflated circular-cylindrical cantilever beam,” AIAA journal, vol. 1, no. 7, pp. 1652–1655, 1963.

[31] V. A. Lubarda, “The mechanics of belt friction revisited,” International Journal of Mechanical Engineering Education, vol. 42, no. 2, pp. 97– 112, 2014.

[32] M. L. Euler, “Remarques sur l’effect du frottement dans l’equilibre,” Mem. Acad. Sci, vol. 18, pp. 265–278, 1762.

[33] D. R. Yoerger, H. Schempf, and D.M. Dipietro, “Design and performance evaluation of an actively compliant underwater manipulator for full-ocean depth.” Journal of Robotic Systems, 8(3), pp. 371-392, 1991.

[34] C.T. Ross, “A conceptual design of an underwater vehicle,” Ocean Engineering, 33(16), pp. 2087-2104, 2006.

[35] G. Yew, A.M. Yusof, Z.M. Ishak, and U. Ishiaku, “Water absorption and enzymatic degradation of poly(lactic acid)/rice starch composites. Polymer Degradation and Stability,” 90(3), pp. 488-500, 2005.